ELSEVIER

Journal of Structural Geology 29 (2007) 159–165

JOURNAL OF STRUCTURAL GEOLOGY

www.elsevier.com/locate/jsg

Cessation of plastic deformation during exhumation of metamorphic tectonites revealed by microboudinage structures

Toshiaki Masuda*, Nozomi Kimura, Atsushi Okamoto, Tomoya Miyake, Yasutomo Omori

Institute of Geosciences, Shizuoka University, 836 Ohya, Shizuoka 422-8529, Japan

Received 1 August 2005; received in revised form 7 June 2006; accepted 30 June 2006
Available online 10 October 2006

Abstract

Microboudinage structures are analysed to examine how quartzose metamorphic tectonites cease plastic deformation during retrograde metamorphism in exhumation. The microboudinage of columnar mineral grains embedded in the quartz matrix record whether plastic deformation ceased as result of the relaxation of differential stress or the plastic–brittle transition of the matrix. The fundamental strain data for microboudinage structures reveal four possible cases in terms of the timing of the plastic–brittle transition in the differential stress history. The classification is closely related to the degree of post-tectonic annealing, which obliterates the microstructures produced during earlier plastic deformation. The approach is applied to three metamorphic tectonites from high-pressure/temperature metamorphic belts, and all are demonstrated to have ceased plastic deformation due to plastic–brittle transition of the matrix, suggesting that the rocks experienced increasing differential stress during exhumation in retrograde metamorphism.

Keywords: Exhumation; Metamorphic rock; Microboudinage; Plastic–brittle transition; Stress history

1. Introduction

Quartz flows plastically under metamorphic pressure-temperature conditions, yet is brittle at shallower crustal levels. Quartz thus experiences a transition from plastic to brittle deformation in the retrograde metamorphic progression during exhumation. Furthermore, under zero differential stress, no plastic deformation can occur even in the plastic regime. The cessation of plastic flow can therefore occur by two modes: the plastic-to-brittle transition, and the relaxation of differential stress. Differentiating between these two modes is essential in microstructural analysis. If cessation by the second mode takes place under metamorphic conditions, the characteristic metamorphic microstructures (e.g., size and shape) of quartz grains formed under the previous regime of plastic deformation will be greatly obliterated during subsequent post-tectonic annealing (e.g., Green et al., 1970; Nam et al., 1999; Tullis, 2002; Passchier and Trouw, 2005). Thus, evaluation of the degree of annealing is critical in microstructural analyses of metamorphic tectonites. However, the influence of such annealing on the microstructures has yet to be evaluated reliably due to a lack of appropriate methods.

This paper proposes a new method for judging which of the two modes of plastic flow cessation is applicable to a sample based on the microboudinage structures of columnar minerals. The method is applied to analysis of the stress and strain history up to the final moment of plastic flow during exhumation for three high-pressure metamorphic rocks.

2. Microboudinage

Microboudinage of a brittle, fibrous mineral grain embedded in a plastic quartz matrix occurs in three stages; pre-fracture deformation (i.e., intact), fracture and separation (Fig. 1). If the applied differential stress is smaller than the fracture strength of the fibrous grain, the grain remains intact

* Corresponding author.
E-mail address: setmasu@ipc.shizuoka.ac.jp (T. Masuda).

0191-8141/$ - see front matter © 2006 Elsevier Ltd. All rights reserved.
doi:10.1016/j.jsg.2006.06.019

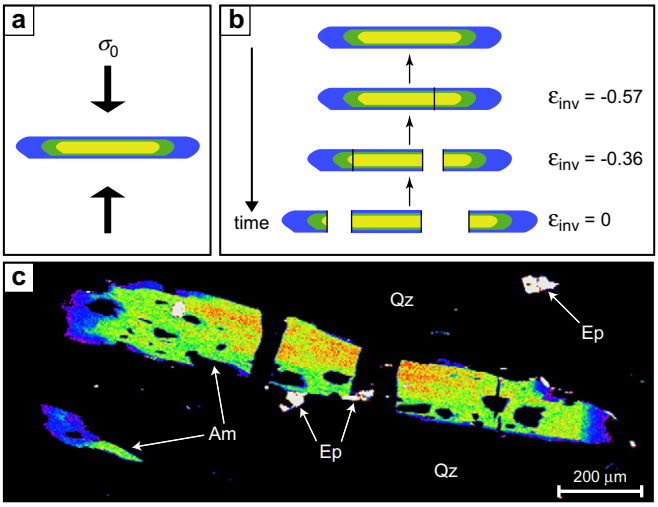

Fig. 1. (a) Schematic of far-field differential stress ($\Delta\sigma$) on microboudins. (b) Schematic of progressive microboudinage with increasing strain. Initial intact grain is restored by the strain reversal method (Ferguson, 1981; Lloyd and Condliffe, 2003). The lower figures show the microstructures that can be seen under optical microscope, and the top figures show the restored intact grain. Attached values of ϵ_{inv} are the strain at which the fracturing occurred. (c) An Al-content map of typical sodic amphibole microboudins embedded in a quartzose matrix (Wakayama, Japan). Qz, quartz; Am, sodic amphibole; Ep, epidote. Al content in sodic amphibole decreases from core to rim, and no overgrowth of amphibole occur at the interboudin gaps. This pattern is much simpler than patterns exemplified by Misch (1969).

while the surrounding matrix flows. As the applied stress becomes equivalent to the fracture strength, the grain fractures to produce two boudins. After fracturing, the two boudins continue to separate passively within the plastically deformed matrix. The new boudins themselves, having larger fracture strengths and requiring larger far-field differential stress to fracture (e.g., Lloyd et al., 1982; Masuda and Kuriyama, 1988; Zhao and Ji, 1997), are then in the pre-fracture stage, and will again undergo fracturing if the differential stress continues to increase.

The fracture strength of fibrous mineral usually differs from grain to grain, and the timing of fracture varies from boudin to boudin (Masuda et al., 2003, 2004c). At any time, the fibrous grains in the matrix will be distributed among three different coexisting groups in the various stages of microboudinage; intact grains, grains undergoing fracture, and fractured grains undergoing separation. The fracture-separation processes thus progresses diachronously.

The accumulation of strain is recorded by an increase in the interboudin gap. The strain reversal method (Ferguson, 1981; Lloyd and Condliffe, 2003) provides the natural-log strain. Fig. 1b shows a schematic of the restoration of microboudinage by the strain reversal method. The inverse natural strain (ϵ_{inv}) is a measure of the partial strain in the period between fracturing and the time at which the quartz matrix ceased to flow (e.g., Masuda et al., 2004b). As the latter time is considered to be synchronised for quartz in all portions in a rock mass, ϵ_{inv} can be used as a measure of the timing of boudin fracture. The inverse natural strain is scaled toward the past and is given as a negative value.

For simplification, the fracture strength of each grain is assumed to be independent of pressure and temperature. Although a slight dependence on pressure and temperature has been reported, the effect is considered to be small (Paterson and Wong, 2005; Kimura et al., 2006).

3. Relationship between magnitude of differential stress and microboudinage

3.1. Fundamental assumptions

For metasedimentary rocks, the focus of the present study, the three trivial boundary conditions for differential stress are as follows: (1) the far-field differential stress applied to sedimentary rocks soon after sea-floor deposition is practically equivalent to zero, (2) rocks undergoing metamorphic plastic deformation experience certain values of the differential stress, and (3) the differential stress applied to rocks exposed at the surface is negligible. The one-dimensional differential stress ($\Delta\sigma$) is assumed to have a single-peak history and to be sufficiently large to drive microboudinage of fibrous minerals (Fig. 2). Stress histories with multiple peaks are dealt with later. The change in differential stress is assumed to be independent of the metamorphic pressure and temperature, and the peak $\Delta\sigma$ is not always synchronized with the peak pressure and temperature of metamorphism.

The transition from plastic to brittle deformation of the matrix minerals is assumed to occur instantaneously at a certain time t_{P-B} during an easing of the temperature and pressure conditions. Four cases are distinguished here based on the temporal relationship between t_{P-B} and specific stages of the stress history (t_S, t_R, t_H, t_E) as shown in Fig. 2.

Fracturing of fibrous minerals is assumed to occur instantaneously when the applied differential stress becomes equivalent to the fracture strength of the fibre (cf., Atkinson, 1987). Fracture strength of many fibres is considered to have a unimodal distribution (e.g., Lawn, 1993; Masuda et al., 2003).

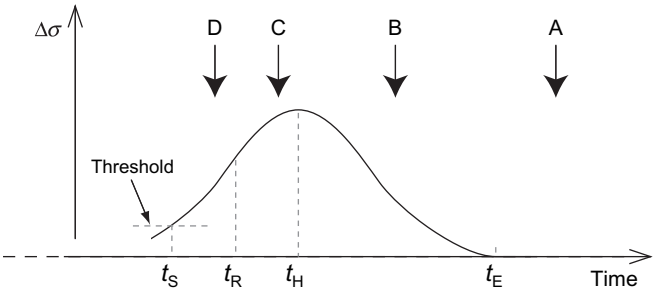

Fig. 2. Schematic of cessation of plastic deformation of matrix mineral. Solid line represents the one-dimensional far-field differential stress ($\Delta\sigma$) with respect to time. The stress exhibits a single-peak history with marker times t_S, t_R, t_H and t_E, denoting the time of threshold of microboudinage, peak-frequency of fracturing, peak $\Delta\sigma$ and $\Delta\sigma = 0$. Arrows (A–D) indicate 4 possible timings of the plastic–brittle transition of the matrix mineral (t_{P-B}). The 4 cases are explained in Figs. 3–6. The peak stress may occur during either prograde or retrograde metamorphism, while the plastic–brittle transition of the matrix takes place during retrograde metamorphism.

3.2. Case A (Fig. 3)

In this case, the plastic–brittle transition of matrix minerals occurs at t_{P-B} after $\Delta\sigma = 0$ is reached (t_E; Fig. 3a). This case represents the typical cessation of plastic flow caused by the relaxation of differential stress. Fracturing of fibrous mineral grains to produce microboudins begins once $\Delta\sigma$ reaches a threshold value (t_S), and the frequency of grain fracture increases with $\Delta\sigma$ up to a maximum (t_R), after which the fracture frequency decreases with increasing $\Delta\sigma$ until no further fracturing occurs (t_H; Fig. 3b). The timing of t_R may be controlled by the maximum population of grains with a certain fracture strength and/or by a rapid increase in $\Delta\sigma$. The microboudins are successively separated after fracturing until $\Delta\sigma = 0$ is reached (t_E).

The fracture–time relationship (Fig. 3b) correlates well with fracture–strain relationship (Fig. 3c). The abscissa of Fig. 3c is the inverse natural strain (ϵ_{inv}) with origin corresponding to the state at which the rock ceases to deform plastically (t_E). The single-peak distribution in Fig. 3b reflects that in Fig. 3c, although the distribution pattern is somewhat skewed due to a change in the strain rate over time. The strain ϵ_S and ϵ_H corresponds to the plastic strain recorded by the microboudins produced at t_S and t_H, respectively.

The temperature and pressure are sufficiently high for the matrix (quartz) to deform in the plastic regime before t_{P-B} and for post-tectonic annealing to act effectively between t_E and t_{P-B}. Post-tectonic annealing in this period will destroy or obliterate the microstructures produced by plastic deformation. Annealing-like processes may also be expected in the period between t_H and t_E with decreasing $\Delta\sigma$.

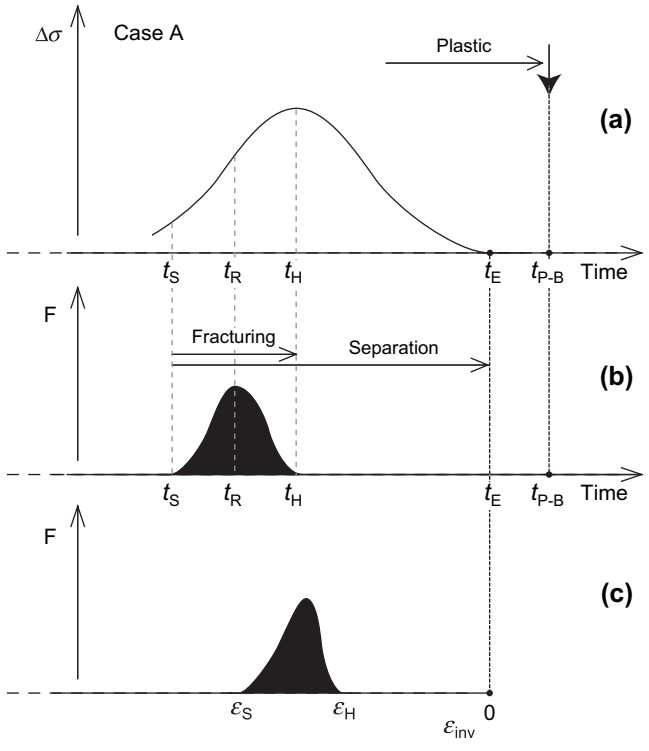

Fig. 3. Case A: $t_E < t_{P-B}$. (a) Stress history. (b) Schematic of microboudin fracture frequency (F) with respect to time. No fracturing occurs after the peak stress is attained at t_H. The frequency distribution is not always symmetric with respect to time. (c) Schematic of fracture frequency (F) with respect to strain. As the strain rate presumably varies throughout microboudinage, the magnitude of ϵ_{inv} is not proportional to time. ϵ_S and ϵ_H are the inverse natural strain recorded by the microboudins produced at t_S and t_H, respectively.

3.3. Case B (Fig. 4)

If the plastic-brittle transition (t_{P-B}) occurs in the period between the peak differential stress (t_H) and $\Delta\sigma = 0$ (t_E), a series of fibrous grain fractures will occur between t_S and t_H. The microboudins produced in this period will be successively separated after t_H until t_{P-B}. The fracture–time and fracture–ϵ_{inv} diagrams for microboudinage under these conditions are shown in Fig. 4b and c. In this case, the strain of final fracturing (ϵ_H) is recorded in the period between the peak $\Delta\sigma$ and the plastic–brittle transition. The resultant fracture–ϵ_{inv} diagram (Fig. 4c) appears schematically different in terms of the position of ϵ_H compared to case A (Fig. 3c). However, as the value of ϵ_H cannot be evaluated quantitatively, the two fracture–ϵ_{inv} diagrams (cases A and B; Figs. 3c and 4c) are practically indistinguishable.

3.4. Case C (Fig. 5)

If the plastic–brittle transition (t_{P-B}) occurs in the period between the peak in fracturing (t_R) and the peak in stress

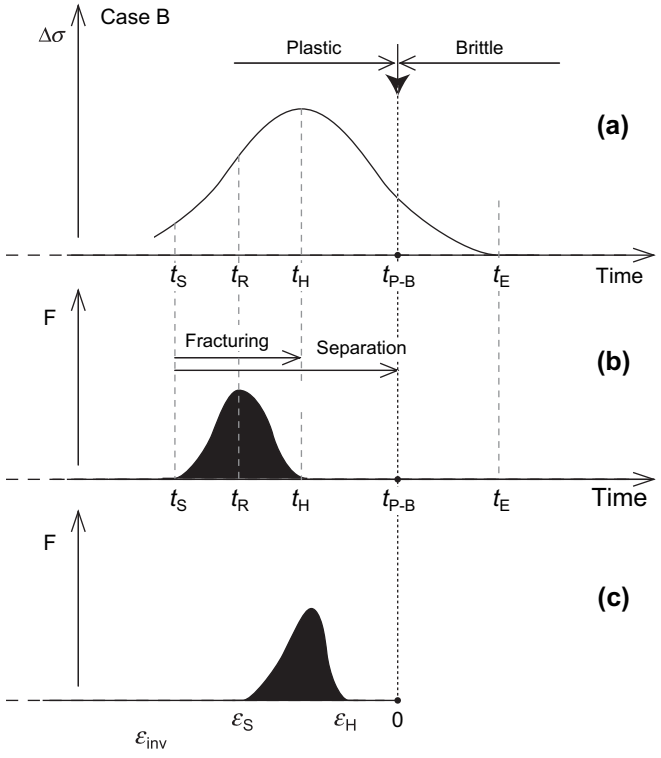

Fig. 4. Case B: $t_H < t_{P-B} < t_E$. (a) Schematic showing the plastic–brittle transition of the matrix between t_H and t_E. (b) Schematic of fracture frequency (F) with respect to time. Fracturing stops at t_H. (c) Schematic of fracture frequency (F) with respect to strain.

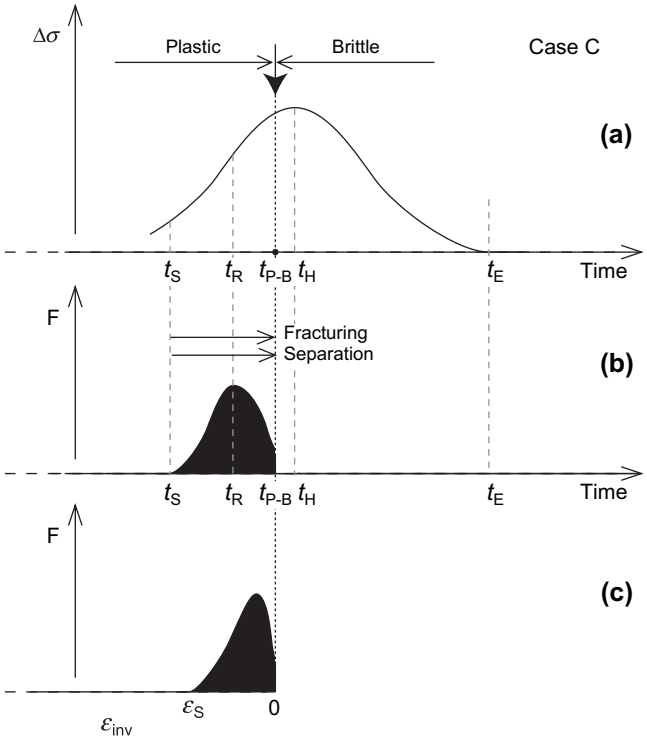

Fig. 5. Case C: $t_R < t_{P-B} < t_H$.

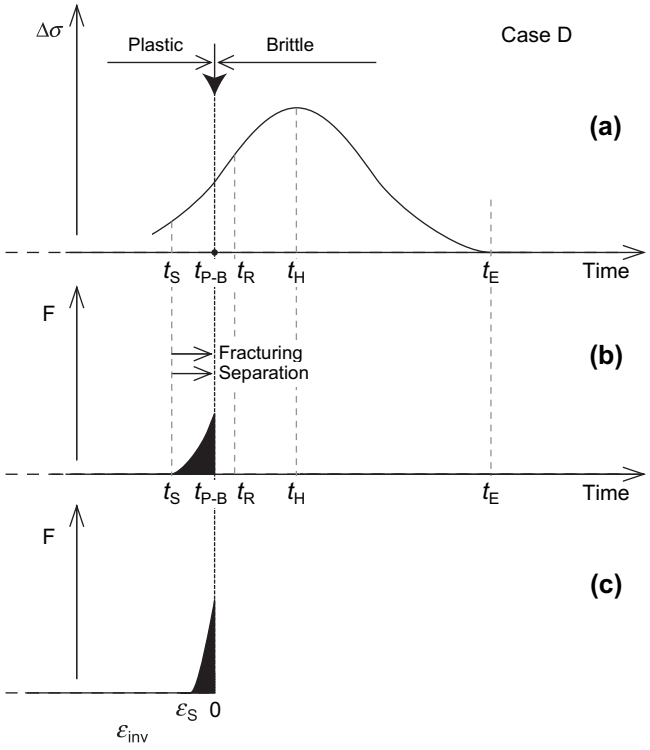

Fig. 6. Case D: $t_S < t_{P-B} < t_R$.

(t_H), the corresponding fracture–time diagram of microboudinage characteristically exhibits fracturing up to the final moment of the plastic–brittle transition (Fig. 5). Thus, the fracture–ϵ_{inv} diagram exhibits a certain frequency of fracturing even at $\epsilon_{inv} = 0$.

3.5. Case D (Fig. 6)

If the plastic–brittle transition takes place before the peak in fracturing (t_R; Fig. 6), the fracture–time diagram exhibits a peak fracture frequency at the time of the plastic–brittle transition (t_{P-B}). The fracture–ϵ_{inv} diagram in this case has a peak at $\epsilon_{inv} = 0$ (Fig. 6c). This case represents one end of the relaxation continuum, corresponding to the abrupt cessation of plastic deformation.

3.6. Differential stress histories with multiple peaks

Consider the case of two local peaks in the differential stress history. If the later differential stress peak is higher and the plastic–brittle transition takes place after the differential stress has been relaxed (t_E), the fracturing of fibrous grains will exhibit two groups of unimodal frequencies with respect to time in the period of plastic deformation of the matrix (Fig. 7). Various fracture–time diagrams will result depending on the timing of the plastic–brittle transition with respect to the two peaks (Fig. 8). If the plastic–brittle transition occurs earlier than E in Fig. 8, the fracture–time and fracture–strain diagrams will appear exactly the same as those with a single-peak history (Figs. 3–6) depending on the timing of the transition to the specific stages of $\Delta\sigma$.

Conversely, if the earlier peak is higher than the later peak, a single unimodal frequency of fracturing with respect to time will result (Fig. 9). The second peak in $\Delta\sigma$ has no influence on the fracturing of the microboudinage and can be ignored. Different timings of the plastic–brittle transition with respect to the $\Delta\sigma$ history therefore produce the same fracture–time and fracture–ϵ_{inv} characteristics considered above for the single-peak history (Figs. 3–6).

If more than three stages of peak differential stress occur in a deformation history, a similar analysis as above is possible based on the fracture–time pattern of microboudinage. The essence of this analysis is the temporal relationship between the plastic–brittle transition and the increase and decrease in differential stress.

4. Application to natural data

Without information on the time and strain rate of plastic deformation, the fracture–time diagrams are not directly obtainable from analysis of natural microboudinage structures. However, the fracture frequency–ϵ_{inv} diagram can be produced using the strain reversal method of Ferguson (1981). Details of the method are discussed in Masuda et al. (2004a,b). Masuda and coworkers (Masuda et al., 1990, 2003, 2004a,b; Masuda and Kimura, 2004) have produced several fracture–ϵ_{inv} diagrams for the microboudinage of piemontite, sodic amphibole and tourmaline from high-pressure/temperature metamorphic rocks, metamorphic sole and a pegmatite body. Three typical diagrams are shown in Fig. 10. The locations and geological settings of these samples can be

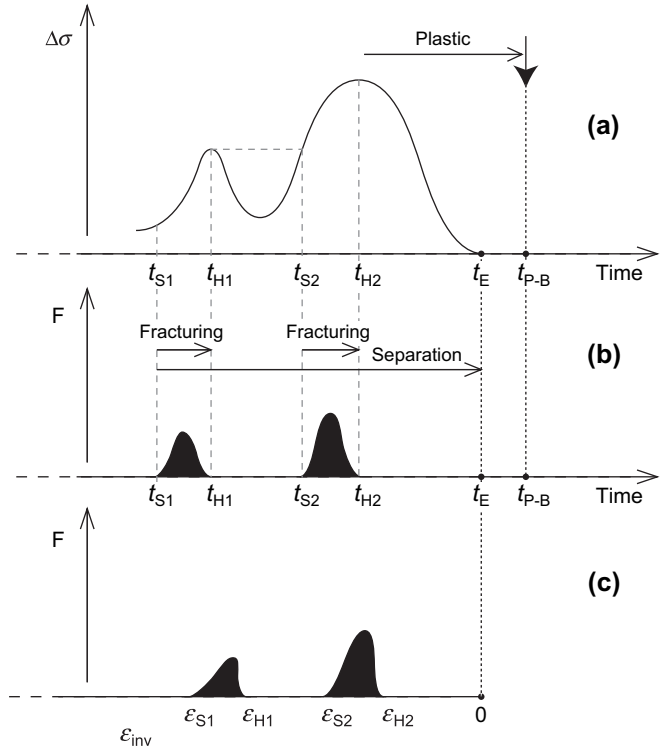

Fig. 7. (a) Two-peak history of differential stress with higher second (later) peak. (b) Two unimodal frequency distributions are recorded with respect to time. Ordinate (F) indicates the frequency of fracturing. The first series of fracturing begins at t_{S1} and ends at t_{H1}, while the second series begins at t_{S2} and ends at t_{H2}. The threshold $\Delta\sigma$ for the second series microboudinage is equivalent to the first peak $\Delta\sigma$. (c) Two unimodal frequency distributions with respect to ϵ_{inv}. ϵ_{S1} etc corresponds to ϵ_{inv} at t_{S1} etc.

found in Masuda et al. (2003, 2004a,b,c). Comparison of these data with the present fracture–ϵ_{inv} diagrams (Figs. 3–9) reveals that such typical natural data can be readily classified into cases C (Eskisehir and Wakayama) and D (Aksu) with a single-peak stress history. This indicates that the plastic–brittle transition of the analysed samples occurred immediately prior to the cessation of plastic flow during a period of increasing differential stress (cf. Lacombe, 2001). Although earlier data presented by Masuda et al. (1990) are classified into Case A or B, these data may be of Case C. After the year 2000 a more precise measurement was developed for very short interboudin gap distances. The short distance presumably influences the frequency of fracturing at very small ϵ_{inv}. Since the frequency pattern at $\epsilon_{inv} = 0$ is the key for the classification, pre-2000 data are considered to be unreliable.

Electronprobe microanalysis (EPMA) of the piemontite and sodic amphibole samples considered here reveals that the chemical zoning patterns of separated microboudins are continuous and that fracturing occurred after near-complete cessation of grain growth (Fig. 1c). This demonstrates that microboudinage occurred in the retrograde stage of metamorphism (Masuda et al., 2004c), which is consistent with the determined timing of microboudinage (cf. for large-scale boudinage, see Mehl et al., 2005).

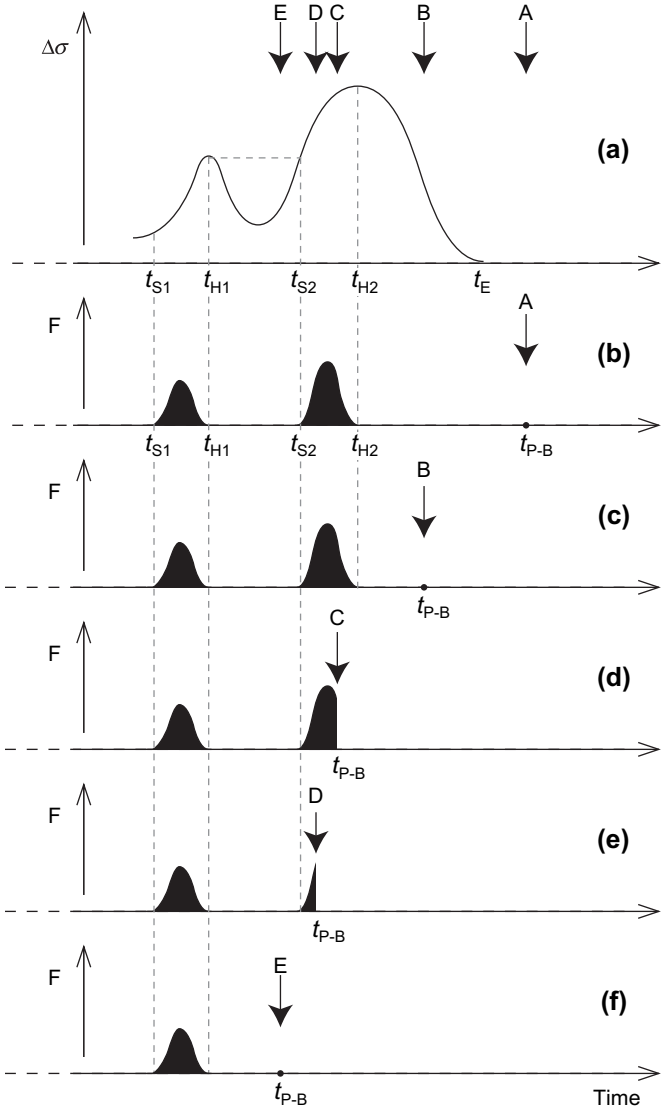

Fig. 8. Two-peak history of differential stress. (a) Timings (A–E) of plastic–brittle transition with respect to the two stress peaks. (b–f) Fracture–time diagrams for the timings A–E. t_{S1} and t_{S2} are the threshold times for $\Delta\sigma$, and t_{H1} and t_{H2} are the times of local peaks in $\Delta\sigma$. Ordinate (F) indicates the frequency of fracturing.

5. Geological implications

5.1. Dynamic exhumation of high-pressure/temperature metamorphic belts

For the examples analysed to date from high-pressure/temperature metamorphic belts (Fig. 10), the cessation of plastic deformation is judged to have occurred as the differential stress was increasing. This suggests the time–$\Delta\sigma$ history shown in Fig. 11, and demonstrates that the exhumation of these rocks occurred under high differential stresses.

Many exhumation models for high-pressure terrains have been proposed based on the *P/T* ratio, the *P–T* path and the exhumation rate determined through metamorphic petrological and geochronological analyses. However, no single mechanism explaining the exhumation of all high-pressure

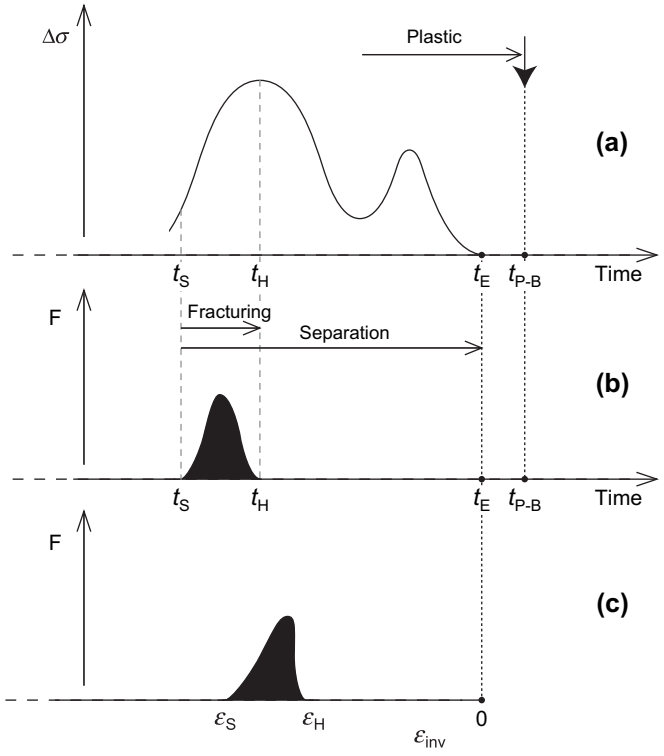

Fig. 9. Two-peak history of differential stress with higher first (earlier) peak.

terrains has been derived (e.g., Platt, 1993; Burov et al., 2001; Pilchin, 2005). Credible models should incorporate increasing differential stress at the plastic–brittle transition of quartz as a key variable, and as such static exhumation models are inappropriate.

The increasing $\Delta\sigma$ regime at the final moment of plastic deformation in high-pressure rocks may appear unusual but is in fact well explained by the law of inertia if it is assumed to be applicable to the plastic deformation of rocks. Plastic deformation is usually expressed as

$$\dot{\epsilon} = A\sigma^n \exp\left(-\frac{Q}{RT}\right) \tag{1}$$

where $\dot{\epsilon}$ is the strain rate, A is a constant, Q is the activation energy, R is the gas constant, T is the absolute temperature, σ is the differential stress (equivalent to $\Delta\sigma$ in this paper) and n is the stress exponent (e.g., Poirier, 1985; Kirby and Kronenberg, 1987; Tullis, 2002). For example, Gleason and Tullis (1995) determined these values experimentally for Black Hills Quartzite ($A = 10^{-4}\ \mathrm{s}^{-1}\ \mathrm{MPa}^{-4}$, $Q = 223$ kJ mol^{-1}, $n = 4$). Equation (1) can be rewritten as

$$\sigma^n = \frac{1}{A}\dot{\epsilon} \exp\left(\frac{Q}{RT}\right). \tag{2}$$

If the inertial movement of a rock body tends to maintain a constant strain rate in all parts of the body with decreasing temperature, the following differential equation can be used to describe the change in differential stress:

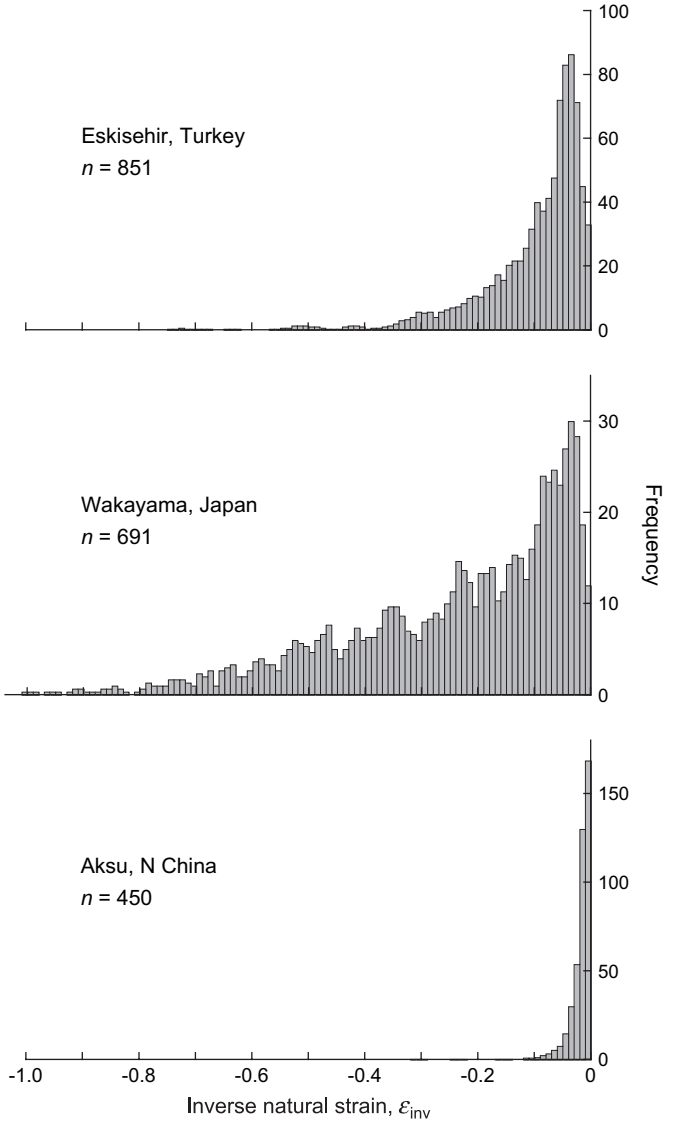

Fig. 10. Measured fracture–ϵ_{inv} data for various high-pressure/metamorphic belts. (a) sodic amphibole from Eskisehir, central Turkey after Masuda et al. (2004b); (b) piemontite from Wakayama, Sambagawa belt, Japan; (c) sodic amphibole from Aksu, NW China after Masuda et al. (2004a). Eskisehir and Wakayama data are classified into case C, while Aksu data is classified into case D with a unimodal history. n, total fracture frequency. Fracture frequency is plotted at 0.01 strain interval. If strain rate is equivalent to $\sim 10^{-14}$/s, the duration of time for the strain interval corresponds to $\sim 10^5$ years. As strain rate is considered not constant, the duration of time varies accordingly.

$$\frac{\partial\sigma^n}{\partial T} = -\frac{Q}{AR}\frac{\dot{\epsilon}}{T^2}\exp\left(\frac{Q}{RT}\right). \tag{3}$$

As the sign of $\partial\sigma^n/\partial T$ is always negative, this equation predicts that decreasing T causes increase in σ, which is consistent with the results in Fig. 11.

5.2. Influence of post-tectonic annealing

Labelling samples as belonging to cases A–D is of primary importance in deformation analysis as the labels suggest the relative degree of obliteration of microstructures in the

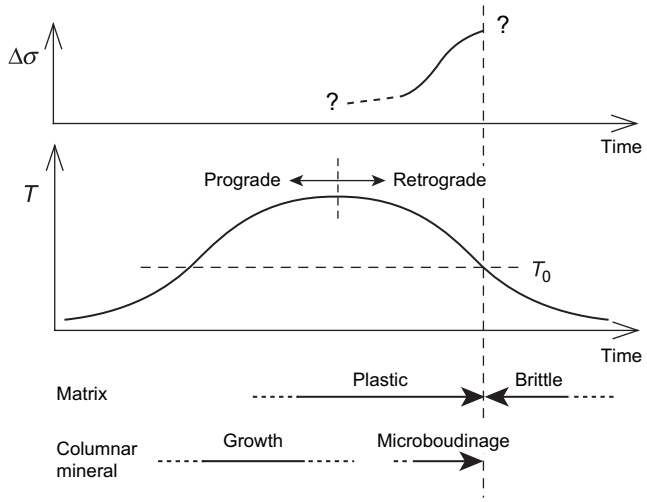

Fig. 11. Schematic history of microboudinage. Horizontal axis = time (t). Temperature (T) increases and decreases during prograde and retrograde metamorphism, respectively. T_0 is the critical temperature above which the matrix mineral (quartz) deforms plastically. Columnar minerals such as sodic amphibole or piemontite grow in the prograde stage, whereas their microboudinage occur in retrograde stage (Masuda et al., 2004c). Case C differential stress ($\Delta\sigma$) history is drawn here. $\Delta\sigma$ increases in the retrograde stage prior to the plastic–brittle transition.

retrograde stage of the metamorphic history. Microstructures of case A samples are considered never to be suitable for deformation analysis due to severe obliteration during annealing after the cessation of plastic deformation. In contrast, microstructures of case D samples are considered to be reliable for deformation analysis because the period of potential obliteration is limited. Reliable deformation analysis can thus only be achieved using reliable microstructures. The inclusion of even a few doubtful data in a set of largely reliable data may have a major impact on the quality of the analysis, and the results of such analyses may be misleading in terms of understanding plastic deformation.

Acknowledgements

The authors are grateful to Hideki Mori for preparing thin sections, Sumio Miyashita and Syoji Arai for encouragement, and Olivier Lacombe and an anonymous reviewer for constructive comments on the manuscript. This work was financially supported in part by the Japanese Society for the Promotion of Science (JSPS).

References

Atkinson, B.K., 1987. Fracture Mechanics of Rock. Academic Press, London.

Burov, E., Jolivet, L., Le Pourhiet, L., Poliakov, A., 2001. A thermomechanical model of exhumation of high pressure (HP) and ultra-high pressure (UHP) metamorphic rocks in Alpine-type collision belts. Tectonophysics 342, 113–136.

Ferguson, C.C., 1981. A strain reversal method for estimating extension from fragmented rigid inclusions. Tectonophysics 79, T43–T52.

Gleason, G.C., Tullis, J., 1995. A flow law for dislocation creep of quartz aggregates determined with the molten salt cell. Tectonophysics 247, 1–23.

Green, H.W., Griggs, D.T., Christie, J.M., 1970. Syntectonic and annealing recrystallization of fine-grained quartz aggregates. In: Paulitsch, P. (Ed.), Experimental and Natural Rock Deformation. Springer, Berlin, pp. 272–335.

Kimura, N., Awaji, H., Okamoto, M., Matsumura, Y., Masuda, T., 2006. Fracture strength of tourmaline and epidote by three-point bending test: application to microboudin method for estimating absolute magnitude of palaeodifferential stress. Journal of Structural Geology 28, 1093–1102.

Kirby, S.H., Kronenberg, A.K., 1987. Rheology of the lithosphere: selected topics. Review of Geophysics 25, 1219–1244.

Lacombe, O., 2001. Paleostress magnitudes associated with development of mountain belts: Insights from tectonic analyses of calcite twins in the Taiwan Foothills. Tectonics 20, 834–849.

Lawn, B., 1993. Fracture of Brittle Solids, second ed. Cambridge University Press, Cambridge.

Lloyd, G.E., Condliffe, E., 2003. 'Strain Reversal': a Windows™ program to determine extensional strain from rigid-brittle layers of inclusions. Journal of Structural Geology 25, 1141–1145.

Lloyd, G.E., Ferguson, C.C., Reading, K., 1982. A stress transfer model for the development of extension fracture boudinage. Journal of Structural Geology 43, 355–372.

Masuda, T., Kimura, N., 2004. Can Newtonian viscous-matrix model be applied to the microboudinage of columnar mineral grains in quartzose metamorphic tectonites? Journal of Structural Geology 26, 1749–1754.

Masuda, T., Kuriyama, M., 1988. Successive "mid-point" fracturing during microboudinage: an estimate of the stress-strain relation during a natural deformation. Tectonophysics 147, 171–177.

Masuda, T., Shibutani, T., Kuriyama, M., Igarashi, T., 1990. Development of microboudinage: an estimate of changing differential stress with increasing strain. Tectonophysics 178, 379–387.

Masuda, T., Kimura, N., Hara, Y., 2003. Progress in microboudin method for palaeo-stress analysis of metamorphic tectonites: application of mathematically refined expression. Tectonophysics 364, 1–8.

Masuda, T., Kimura, N., Fu, B., Li, X., 2004a. Validity of the microboudin method for palaeo-stress analysis: application to extraordinarily long sodic amphibole grains in a metachert from Aksu, China. Journal of Structural Geology 26, 203–206.

Masuda, T., Nakayama, S., Kimura, N., Onodera, K., Okamoto, A., 2004b. Triaxial stress state deep in orogenic belts: an example from Turkey. Journal of Structural Geology 26, 2203–2209.

Masuda, T., Shibutani, T., Ochiai, T., Akagi, S., Yamaguchi, H., Kugimiya, Y., Kimura, N., Miyake, T., 2004c. Microboudin structures of piemontite along the Sambagawa metamorphic belt, Japan: implications for lateral variation of differential stress during regional metamorphism. Journal of Metamorphic Geology 22, 199–205.

Mehl, C., Jolivet, L., Lacombe, O., 2005. From ductile to brittle: evolution and localization of deformation below a crustal detachment (Tinos, Cyclades, Greece). Tectonics 24, TC4017, doi:10.1029/2004TC001767.

Misch, P., 1969. Paracrystalline microboudinage of zoned grains and other criteria for synkinematic growth of metamorphic minerals. American Journal of Science 267, 43–63.

Nam, T.N., Otoh, S., Masuda, T., 1999. In-situ experiments of octachloropropane as a rock analogue: kinetics and energetics of grain growth. Tectonophysics 304, 57–70.

Passchier, C.W., Trouw, R.A.J., 2005. Microtectonics, second ed. Springer-Verlag, Berlin.

Paterson, M.S., Wong, T., 2005. Experimental Rock Deformation—The Brittle Field, second ed. Springer-Verlag, Berlin.

Pilchin, A., 2005. The role of serpentinization in exhumation of high- to ultra-high-pressure metamorphic rocks. Earth and Planetary Science Letters 237, 815–828.

Platt, J.P., 1993. Exhumation of high-pressure rocks: a review of concepts and processes. Terra Nova 5, 119–133.

Poirier, J.-P., 1985. Creep of Crystals. Cambridge University Press, Cambridge, 260 p.

Tullis, J., 2002. Deformation of granitic rocks: Experimental studies and natural examples. In: Karato, S., Wenk, H.-W. (Eds.), Plastic Deformation of Minerals and Rocks. Reviews in Mineralogy and Geochemistry 51, pp. 51–95.

Zhao, P., Ji, S., 1997. Refinements of shear-lag model and its applications. Tectonophysics 279, 37–53.